

# Spin Liquid Ground State of the Spin- $\frac{1}{2}$ Square $J_1$ - $J_2$ Heisenberg Model

Hong-Chen Jiang

*Kavli Institute for Theoretical Physics, University of California, Santa Barbara, CA 93106 and  
Center for Quantum Information, IIS, Tsinghua University, Beijing, 100084, China*

Hong Yao

*Department of Physics, Stanford University, Stanford, CA 94305, USA and  
Institute for Advanced Study, Tsinghua University, Beijing, 100084, China*

Leon Balents

*Kavli Institute for Theoretical Physics, University of California, Santa Barbara, CA 93106  
(Dated: March 3, 2018)*

We perform highly accurate density matrix renormalization group (DMRG) simulations to investigate the ground state properties of the spin- $\frac{1}{2}$  antiferromagnetic square lattice Heisenberg  $J_1$ - $J_2$  model. Based on studies of numerous long cylinders with circumferences of up to 14 lattice spacings, we obtain strong evidence for a topological quantum spin liquid state in the region  $0.41 \leq J_2/J_1 \leq 0.62$ , separating conventional Néel and striped antiferromagnetic states for smaller and larger  $J_2/J_1$ , respectively. The quantum spin liquid is characterized numerically by the absence of magnetic or valence bond solid order, and non-zero singlet and triplet energy gaps. Furthermore, we positively identify its topological nature by measuring a non-zero topological entanglement entropy  $\gamma = 0.70 \pm 0.02$ , extremely close to  $\gamma = \ln(2) \approx 0.69$  (expected for a  $Z_2$  quantum spin liquid) and a non-trivial finite size dimerization effect depending upon the parity of the circumference of the cylinder. We also point out that a valence bond solid, and indeed any discrete symmetry breaking state, would be expected to show a constant correction to the entanglement entropy of *opposite* sign to the topological entanglement entropy.

PACS numbers: 75.10.Jm, 75.50.Ee, 75.40.Mg

## I. INTRODUCTION

Quantum spin liquids (QSLs) are elusive magnets without magnetism, resisting symmetry breaking even at zero temperature due to strong quantum fluctuations and geometric frustration<sup>1</sup>. The simplest QSLs known theoretically are characterized by topological order<sup>2-4</sup>, and support fractionalized excitations including spinons, which carry the spin (1/2) but not the charge of the electron. Since the QSL state was suggested by Anderson<sup>5</sup>, it has been sought, mostly unsuccessfully, in models and materials. However, exciting indications of QSL ground states were recently reported in numerical studies of models on the honeycomb<sup>6</sup> and kagome<sup>7</sup> lattices. Here we report strong evidence for a QSL state in the square lattice  $J_1$ - $J_2$  antiferromagnetic (AFM) Heisenberg model, with the Hamiltonian

$$H = J_1 \sum_{\langle ij \rangle} \mathbf{S}_i \cdot \mathbf{S}_j + J_2 \sum_{\langle\langle ij \rangle\rangle} \mathbf{S}_i \cdot \mathbf{S}_j, \quad (1)$$

where  $\mathbf{S}_i$  is the spin-1/2 operator on site  $i$  and  $\langle ij \rangle$  ( $\langle\langle ij \rangle\rangle$ ) denotes nearest neighbors (next nearest neighbors). In the following we set  $J_1 = 1$  as the unit of energy, and consider only the frustrated case  $J_2 > 0$ .

Eq. (1) is of fundamental interest for its simplicity, and for its relevance to cuprates, Fe-based superconductors<sup>8-12</sup>, and other materials<sup>13</sup>. Accordingly, it is among the most studied models in frustrated quantum magnetism<sup>14-25</sup>. These previous studies have established the existence of a non-magnetic ground state between the Néel and striped AFM states which occur for small and large  $J_2$ , respectively.

To characterize the non-magnetic phase, we can ask two main types of questions. First, we may ask about its symmetries. Being non-magnetic, the ground state retains the internal SU(2) spin-rotation invariance, but it may break spatial ones. If SU(2) is preserved but spatial symmetries are broken in such a way that the unit cell is enlarged, the system is said to have valence bond solid (VBS) order. Second, we may ask about the range of entanglement of the wavefunction. The simplest representative wavefunctions for VBS states are continuously deformable by local unitary transformations into product states. Such is true for typical ground state wavefunctions for systems with broken discrete symmetries (the space group of a lattice is discrete). As such, these wavefunctions have only short-range entanglement (Schrödinger cat states are possible in finite systems and will be discussed in Sec. IV). Wavefunctions which *cannot* be continuously transformed in this way into product states may be said to exhibit *long-range entanglement*. This is true for all gapless critical phases, as well as for some gapped states. In particular, gapped QSL states exhibit a particularly simple type of long-range entanglement, characterized by *Topological Entanglement Entropy* (TEE)<sup>26,27</sup>. Often the two types of characterization are conflated, but this is not necessarily the case. States with both long range entanglement, e.g. with TEE, and VBS order exist. Such states, while not technically QSLs by the standard definition given above, have all the same exotic physics as QSLs with unbroken spatial symmetry. We note, however, that it is believed that for S=1/2 spins on a lattice such as this one with an odd number of spins per unit cell, the *absence* of VBS order *implies* the presence of long-range entanglement. Therefore a

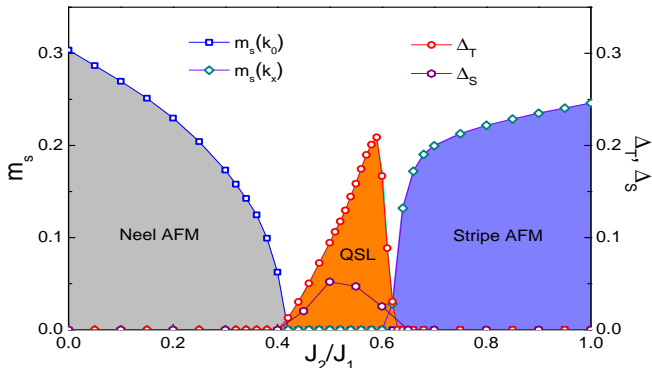


FIG. 1: (Color online) The ground state phase diagram for the spin- $\frac{1}{2}$  AFM Heisenberg  $J_1$ - $J_2$  model on the square lattice, as determined by accurate DMRG calculations on long cylinders with  $L_y$  up to 14. Changing the coupling parameter  $J_2/J_1$ , three different phases are found: Néel antiferromagnet (AFM), topological quantum spin liquid (QSL), and stripe AFM phase.  $m_s(\mathbf{k}_0 = (\pi, \pi))$  [ $m_s(\mathbf{k}_x = (\pi, 0))$ ] denotes the staggered magnetization in the Néel AFM phase [stripe AFM phase], whose saturation value is  $1/2$ .  $\Delta_S$  and  $\Delta_T$  denote the spin singlet gap and spin triplet gap, respectively.

convincing demonstration of vanishing VBS order does, indirectly, imply interesting QSL physics. It is, however, less important to characterize and proving the existence of a QSL than positive, direct evidence of long-range entanglement.

Most of the literature on the intermediate phase of the  $J_1$ - $J_2$  model has focused on the possibility of symmetry breaking VBS order. Many of these prior studies have suggested that the intermediate state has VBS order. We note, however, that all numerical results for the  $J_1$ - $J_2$  model are based either on biased techniques (such as series expansion or coupled cluster methods, or fixed node or related versions of Monte Carlo adapted to avoid the sign problem which is present for unbiased Monte Carlo in this system), or on exact diagonalization of very small systems. Some *theoretical* motivation for the possibility of VBS order comes from the theory of deconfined quantum criticality<sup>28</sup>, which predicts that a continuous quantum phase transition – a deconfined quantum critical point (DQCP) – should occur between an ordered Néel state and a plaquette or columnar VBS state, *in some models*. However, the existence of such a transition does not in any way imply that it occurs for the  $J_1$ - $J_2$  model in question, or that this particular model even harbors a VBS phase. Other theoretical motivation for VBS order comes from its presence in some large- $N$  generalizations of the nearest-neighbor Heisenberg antiferromagnet. However, these large  $N$  studies are not controllably close to the  $SU(2)$  case and moreover do not consider second neighbor interactions. In short, we believe there is very little compelling evidence for the existence of VBS order in the isotropic  $S = 1/2$   $J_1$ - $J_2$  model to be found in the prior literature. We will return to discuss VBS states in Sec. VIA.

The *only* unbiased technique capable of treating generic frustrated two dimensional spin systems of moderately large size is the Density Matrix Renormalization Group (DMRG)

method.<sup>7,29–31</sup> While the sizes that can be studied using the DMRG are not as large as those accessible by quantum Monte Carlo (QMC) for *unfrustrated* models, they are still very large and they are not limited by the sign problem, which prevents application of QMC to most realistic physical models. Moreover, the DMRG has some advantages over QMC: it is intrinsically a zero temperature technique, and obtains a convenient representation of the ground state wavefunction. Most importantly for our purposes, the DMRG is very efficient and convenient for calculating the entanglement entropy, which we return to in some detail below. In this paper, we report the results of extensive simulations (with truncation error  $\sim 10^{-7}$ ) on numerous cylinders of circumference  $L_y = 3 - 14$ , and lengths  $L_x \geq 2L_y$ . In our simulations, we measure spin-spin correlation functions, correlation functions and expectation values of VBS order parameters, bulk singlet and triplet energy gaps, and entanglement entropy. All results confirm the existence of magnetic order for small and large  $J_2$ , and that (see Fig. 1) the ground state for  $0.41 \leq J_2/J_1 \leq 0.62$  is non-magnetic, in very good agreement with the most accurate prior results from series expansion and coupled cluster<sup>24</sup> methods. Furthermore, we find that the intermediate phase has a gap to both singlet and triplet excitations and, within our uncertainty, *no* VBS order in the 2D limit as extrapolated from the VBS correlation functions. We carry out further checks for possible finite-size effects due to the boundaries, to see if this might artificially suppress VBS order, and see no indication that this is the case.

The latter results suggests a QSL state, based on negative evidence: the apparent absence of VBS order. We find two *positive* evidences that this suggestion is correct, and that the state is a  $Z_2$  QSL. First, we find a non-zero TEE,  $\gamma$ , which is a constant and universal *reduction* of the von Neumann entanglement entropy, known to vanish in any gapped state with short-range entanglement. Notably, we point out in Sec. IV that discrete spontaneous symmetry breaking phases such as valence bond solids have absolute ground states which are Schrödinger cat states with a constant *enhancement* of the entanglement entropy – i.e. an effect of *opposite sign* to the TEE. Phases with non-zero  $\gamma$  and a gap to all excitations are *topological phases*. Like conformal field theories in two dimensions, only discrete types of topological phases exist, with discrete allowed values of  $\gamma$  (which plays a role somewhat similar to the central charge in a conformal field theory). For all points we have studied within the non-magnetic phase, the value of  $\gamma$  is equal, within numerical uncertainty of 2%, to  $\ln(2)$ , which is the *minimal* value possible for  $\gamma$  in a topological phase with time-reversal symmetry. A topological entanglement entropy of  $\gamma = \ln(2)$  implies either a  $Z_2$  QSL or a “doubled semion” phase<sup>37</sup>. As there is, to our knowledge, no theory suggesting the appearance of the semion phase in an  $SU(2)$  invariant spin-1/2 model, we take this as strong evidence for a  $Z_2$  QSL state. The second positive evidence for a  $Z_2$  QSL is a remarkable odd/even effect, in which static VBS order is entirely absent for even  $L_y$  but is observed directly in the VBS expectation values for odd  $L_y$ . This is expected on general theoretical grounds for a  $Z_2$  QSL, as we show in Appendix A 1. We compare the behavior of the numerically observed static VBS order for odd circumference cylinders with

theory, and find quite consistent results.

The remainder of the paper is organized as follows. In Sec. II, we report results of magnetic and dimer correlation functions, and their extrapolation to the infinite system limit. Sec. III discusses the singlet and triplet energy gaps. Sec. IV describes the theory and measurements of the topological entanglement entropy, and Sec. V presents results on the even-odd effect. We conclude in Sec. VI with a summary of the conclusions, and a detailed discussion of the reasons to think VBS order, even weak, is unlikely in this model, in response to a recent critique.<sup>32</sup> The Appendix gives a theoretical derivation and discussion of some properties of  $Z_2$  quantum spin liquids.

## II. CORRELATION FUNCTIONS

In this section we discuss the behavior of correlation functions of spin and dimer (VBS) operators. Here and in the rest of the paper, all our numerical data is based on DMRG simulations on cylinders, i.e. finite square lattices with  $N = L_x \times L_y$  sites and with open and periodic boundary conditions in the  $x$  and  $y$  directions, respectively. When not otherwise specified, we fix the aspect ratio to  $L_x/L_y = 2$ , with  $L_y = L$ , then  $L_x = 2L$ , which has been shown to optimize results in the DMRG<sup>7,30,31</sup>. Moreover, to extract bulk properties, we will often work on the central half of the system with an effective system size  $N_c = L \times L$ . For instance, in computing spin correlation functions  $\langle \mathbf{S}_i \cdot \mathbf{S}_j \rangle$ , we restrict site indices  $i$  and  $j$  to the central half of the system so that the obtained correlation functions could represent the bulk properties. We keep more than  $m = 12000$  states in each DMRG block for most systems, which is found to give excellent convergence with truncation errors of the order or less than  $10^{-7}$ .

We begin with measurements of the magnetic correlations in the ground state,  $\langle \mathbf{S}_i \cdot \mathbf{S}_j \rangle$ , and the corresponding static structure factor  $M_s(\mathbf{k}, L) = \frac{1}{L^2} \sum_{ij} e^{i\mathbf{k} \cdot (\mathbf{r}_i - \mathbf{r}_j)} \langle \mathbf{S}_i \cdot \mathbf{S}_j \rangle$ . The structure factor is peaked at  $\mathbf{k}_0 = (\pi, \pi)$  for small  $J_2$  and  $\mathbf{k}_x = (\pi, 0)$  or  $\mathbf{k}_y = (0, \pi)$  for large  $J_2$ , corresponding to the Néel and striped AFM states, respectively. To quantitatively analyze the order, we perform an extrapolation of the (squared) staggered magnetization,  $m_s^2(\mathbf{k}, L) = \frac{1}{L^2} M_s(\mathbf{k}, L)$ , to the two dimensional limit ( $L = \infty$ ) according to the generally accepted form  $m_s^2(\mathbf{k}, L) = m_s^2(\mathbf{k}, \infty) + \frac{a}{L} + \frac{b}{L^2}$  (see Figs.2(a) and (b)).

Extrapolation from data for  $L \leq 12$  shows that the Néel AFM order is non-zero for  $J_2 < 0.41$ , while striped AFM order onsets for  $J_2 > 0.62$ , thus establishing the phase boundaries shown in Fig. 1. A strong check on the quality of our results is the staggered magnetization at  $J_2 = 0$ , which we find to be  $m_s(\mathbf{k}_0, \infty) = 0.304$ , very close to the best known numerical value of the magnetic moment  $m_s = 0.307$  by large-scale quantum Monte-Carlo (QMC) simulation<sup>33</sup>. The location of the phase boundaries is consistent with previous studies<sup>25,34</sup>.

We next consider possible VBS order, which has been considered a prime candidate for non-magnetic symmetry breaking in the intermediate phase. From the bond operators  $B_i^\alpha \equiv \mathbf{S}_i \cdot \mathbf{S}_{i+\alpha}$  on bond  $(i, i + \alpha)$  with

$\alpha = \hat{x}$  or  $\hat{y}$ , we define the dimer-dimer correlation functions  $\langle B_i^\alpha B_j^\beta \rangle$ , with the corresponding structure factor  $M_d^{\alpha\beta}(\mathbf{k}, L) = \frac{1}{L^2} \sum_{ij} e^{i\mathbf{k} \cdot (\mathbf{r}_i - \mathbf{r}_j)} \left( \langle B_i^\alpha B_j^\beta \rangle - \langle B_i^\alpha \rangle \langle B_j^\beta \rangle \right)$ . Typical VBS patterns expected theoretically have momentum  $\mathbf{k}_x = (\pi, 0)$  or  $\mathbf{k}_y = (0, \pi)$ , so to study the correlations, we focus on  $L_y$  even, for which  $k_y = \pi$  is an allowed momentum. We indeed observe a maximum in  $M_d^{aa}(\mathbf{k}, L)$  at  $\mathbf{k} = \mathbf{k}_a$  ( $a = x, y$ ), and therefore define the dimer order parameters by  $m_{d,a}^2(L) = \frac{1}{L^2} M_d^{aa}(\mathbf{k}_a, L)$ . As shown in the inset of Fig.3, for finite systems, both horizontal and vertical dimer order parameters have a maximum within the intermediate phase. Note that for the larger systems, the order parameters for horizontal and vertical dimers become nearly indistinguishable, indicating that the isotropy of the two dimensional limit is being recovered.

Applying the same extrapolation scheme used for the magnetic order parameters, however, the extrapolated dimerization  $m_{d,a}^2$  (see Fig.4(a)) for  $L \rightarrow \infty$  vanishes for all  $0 \leq J_2 \leq 1$ . For characteristic values of  $J_2$  near the middle of the intermediate phase, an exponential fit of the dimer-dimer correlation function (not shown) gives an estimate of the VBS correlation length  $\xi_d \approx 4$ . Taken at face value, these observations indicate that the VBS order is a finite-size effect, and vanishes in the thermodynamic limit. More conservatively, at a minimum, the result indicates that the VBS correlations we observe cannot be distinguished from just *fluctuation* effects in a state with unbroken spatial symmetry, and there is no a priori reason to regard them as evidence of true VBS order.

Both columnar and plaquette VBS phases have been suggested in the past. The complex order parameter  $m_{d,x} + im_{d,y}$  in fact is sufficient to detect and distinguish both columnar and plaquette VBS phases<sup>28</sup>, but as an additional check we measure directly the correlations of the plaquette operator  $P_i = \frac{1}{2}(\Pi_i + \Pi_i^{-1})$  where  $\Pi_i$  cyclically permutes the four spins of the plaquette  $i$  in a clockwise fashion. The plaquette order parameter determined from the corresponding structure factor (see Supplementary Information) is shown in Fig. 4(b). Like the VBS order parameter, it vanishes in the extrapolation to the thermodynamic limit.

## III. ENERGY GAPS

We next consider the energy gap to bulk singlet and triplet excited states, and find both to be non-zero in the intermediate phase. This rules out *any* type of magnetic order, not just the  $(\pi, \pi)$  and  $(\pi, 0)$  orders considered explicitly via the correlation functions. It also rules out other exotic states breaking SU(2) symmetry, such as spin nematics. This is because any state with broken spin-rotational symmetry must have a vanishing gap by Goldstone's theorem.

To obtain *bulk* excited states, we follow Refs. 7,30,31, and first target only one state, sweeping enough to obtain a high-accuracy ground state; then we restrict the range of bonds that are updated in the DMRG sweeps to the central half of the sample and target the two lowest-energy states, again sweeping to high accuracy, but keeping the end regions of

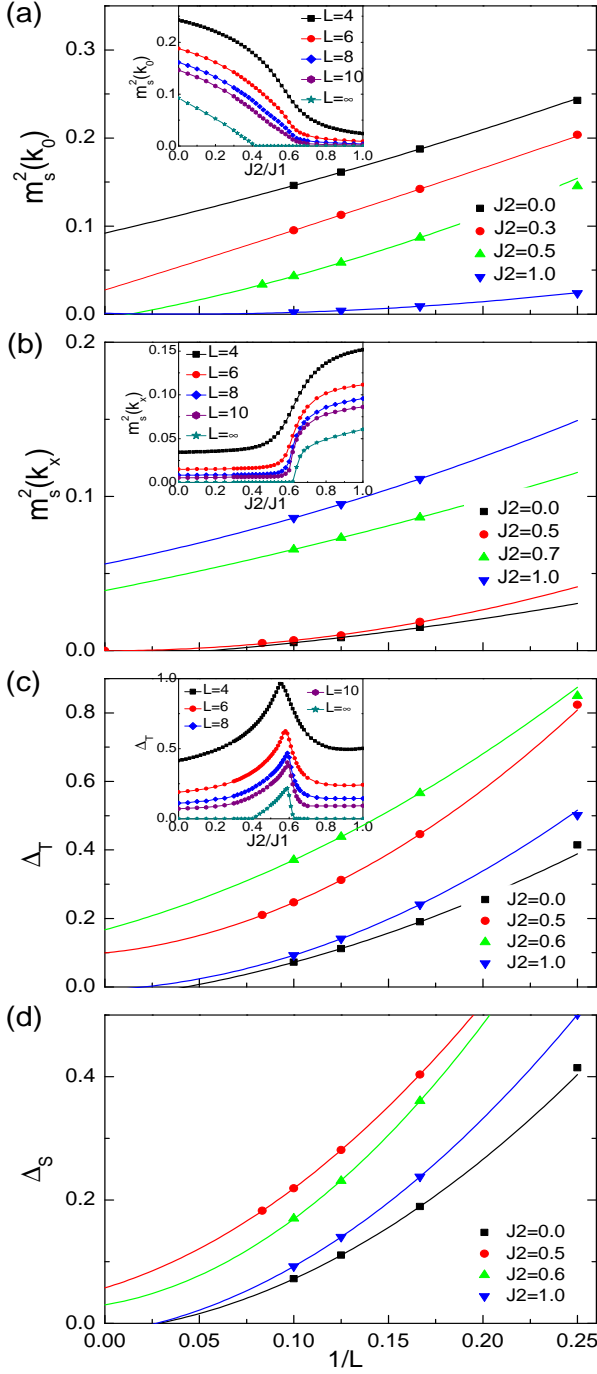


FIG. 2: (Color online) Finite-size extrapolations of the magnetic order parameters and spin excitation gaps. (a) The Néel AFM order parameter  $m_s^2(\mathbf{k})$  at wavevector  $\mathbf{k}_0 = (\pi, \pi)$  and (b) stripe AFM order parameter  $m_s^2(\mathbf{k})$  at wavevector  $\mathbf{k}_x = (\pi, 0)$  or  $\mathbf{k}_y = (0, \pi)$ , for various values of  $J_2$ , fitted using second-order polynomials in  $1/L$ . Néel AFM order disappears for  $J_2 > 0.41$ , while stripe AFM order develops for  $J_2 > 0.62$ , as seen in the corresponding insets. (c) Spin triplet gap  $\Delta_T$  and (d) spin singlet gap  $\Delta_S$  for different values of  $J_2$ , also fitted using second-order polynomials in  $1/L$ . The inset in (c) shows  $\Delta_T$  for  $L = 4, 6, 8, 10$ , and the extrapolated values in the 2D limit, as functions of  $J_2$ . For the spin singlet gap, due to the numerical cost, we focus on several typical data points as shown in (d).

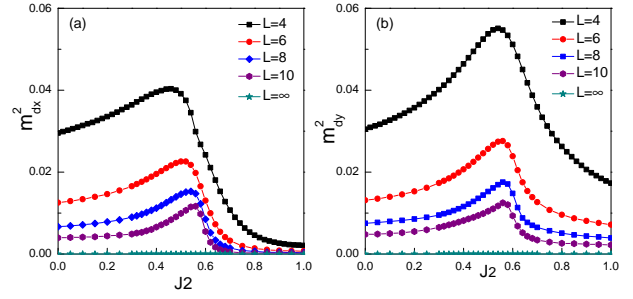


FIG. 3: (Color online) Order parameters for horizontal and vertical dimers. (a) The dimer order parameter  $m_{d,x}^2$  at wavevector  $\mathbf{k}_x = (\pi, 0)$  and (b) plaquette order parameter  $m_{d,y}^2$  at  $\mathbf{k}_y = (0, \pi)$ , as a function of  $J_2$  for different system sizes, and extrapolated to  $L = \infty$ .

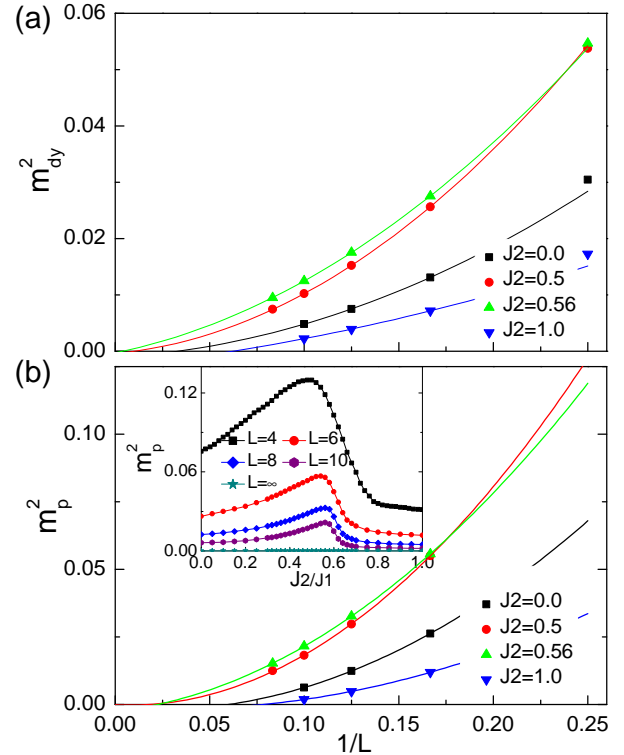


FIG. 4: (Color online) Finite-size extrapolations of the dimer order parameter and plaquette order parameter. (a) The dimer order parameter  $m_{d,y}^2$  at wavevector  $\mathbf{k}_y = (0, \pi)$  and (b) plaquette order parameter  $m_p^2$ , for various values of  $J_2$ , fitted using second-order polynomials in  $1/L$ . The inset shows the plaquette order parameter for  $L = 4, 6, 8, 10$ , and the extrapolated values in the 2D limit, as functions of  $J_2$ .

the samples locally in the ground state. To obtain the spin triplet gap, we do similar things, but target states with total  $S_z = 0$  and  $S_z = 1$  separately. As for the staggered magnetization, we perform a second order polynomial extrapolation of the singlet and triplet gaps to the thermodynamic limit (Figs. 2(c,d)). Consistent with expectation, both  $\Delta_S(L = \infty)$  and  $\Delta_T(L = \infty)$  vanish in the two AFM phases. They are

both, however, non-zero and large in the intervening region (see Fig. 1). This rules out any state with broken SU(2) spin symmetry.

We notice that the singlet gap remains consistently below the triplet gap throughout the intermediate phase. This is an indication of short-range singlet formation. It is consistent with a spin liquid state, and with a system with weak VBS order. We would, however, expect a strong VBS state to have a triplon excitation, corresponding to breaking one singlet bond, as the lowest energy bulk excitation, lower than singlet excitations which require breaking two singlets. So we can exclude a strong VBS state in this sense based on the excitation spectrum.

#### IV. TOPOLOGICAL ENTANGLEMENT ENTROPY

The above results provide evidence *against* conventional ordering in the intermediate region. Magnetic ordering appears comfortably excluded by both the correlation function and excitation spectrum analysis. Extrapolation of the dimer correlations to the thermodynamic limit argues that VBS order is absent as well, but we cannot exclude some very weak ordering on these grounds alone.

We now undertake a *positive* evidence for a QSL with topological order – the topological entanglement entropy. The topological entanglement entropy is obtained from the von Neumann entanglement entropy  $S(A)$ . The latter is defined for a state  $|\psi_0\rangle$  (which we take to be the ground state) and a partition of the full system into a subsystem  $A$  and its complement  $B$ , by first constructing the reduced density matrix  $\rho_A = \text{Tr}_B |\psi_0\rangle\langle\psi_0|$ . Then the entanglement entropy  $S(A) = -\text{Tr}_A(\rho_A \ln \rho_A)$ . For a system with a gap to all bulk excitations (as we have verified in Sec. III), provided the boundary between  $A$  and  $B$  is taken to be smooth (i.e. have no corners), the entanglement entropy must scale according to

$$S(A) \sim \sigma L - \gamma + \dots, \quad (2)$$

where the omitted terms vanish in the large  $L$  limit. Here  $\sigma$  is a non-universal number that measures the local entanglement across the boundary. According to Refs. 26,27, the *positive* term  $\gamma$  is *universal* constant reduction from the area law.<sup>26,27</sup> It arises entirely from non-local entanglement, and is topological in origin. In particular, the area law is *strictly* obeyed, i.e.  $\gamma = 0$ , for any state without long-range entanglement, that is, which can be smoothly deformed into a product state. This is true, in the absence of spontaneously broken symmetry, for any ground state which does not exhibit topological order, i.e. which is not a topological QSL.<sup>26,27</sup>

Although it is not discussed in the seminal papers on topological entanglement entropy, a non-zero *negative*  $\gamma$  (i.e. a positive correction to the area law) *can* arise from discrete spontaneous symmetry breaking (more severe positive corrections to the area law arise in the case of a continuous broken symmetry,<sup>35,36</sup> but this is inconsistent with the existence of a gap to bulk excitations). In particular, in an ideal model with an exact discrete symmetry of the Hamiltonian, the eigenstates must form irreducible representations of the symmetry

group. For simple abelian groups such as  $Z_N$ , these representations are one dimensional, so this implies the Hamiltonian eigenstates are mutual eigenstates of the symmetry generators. This applies of course to the absolute ground state of the system, which is therefore a Schrödinger cat state, which superimposes the symmetry broken global ground states with equal weight. For the case of a fully broken  $Z_N$  symmetry, with  $N$  degenerate ground states in the thermodynamic limit, this gives rise to  $N$  terms in the Schmidt decomposition of the ground state, and therefore a correction  $\gamma = -\ln(N)$ , i.e. a positive correction to the area law or  $\ln(N)$ . We have indeed observed such behavior numerically in test studies of the simplest quantum transverse field Ising model in the ferromagnetic phase, consistent with the expected  $\gamma = -\ln(2)$  for this case.

Thus we see that there are two potential sources of a non-zero constant term in the entanglement entropy. A topological contribution which *decreases* the entropy, and a symmetry breaking contribution which *increases* it. The latter correction arises from *global* entanglement of the entire system. In work completed since the earlier version of this article appeared,<sup>37</sup> it has been shown that the DMRG, which is a minimum entanglement approximation, tends to converge, for large systems, to quasi-ground states which capture all entanglement out to a long length scale, but not the last global entanglement. That is, for long systems, the convergence of the DMRG is first to a *Minimum Entanglement State* (MES) amongst the manifold of states comprising the degenerate ground states in the thermodynamic limit<sup>37</sup>. For topologically ordered phases, which have a ground state degeneracy in the thermodynamic limit of topological origin, the MES exhibits the universal reduction of entanglement entropy, i.e. the universal positive value of  $\gamma$ . For symmetry broken states, for which there is a ground state degeneracy in the thermodynamic limit dictated by symmetry, the MES is simply a single product-like state, with  $\gamma = 0$ . As shown by Jiang, Wang and Balents in Ref. 37, for a fixed system size which is not too large, the DMRG can be pushed to converge to the global ground state, by increasing the number of states  $m$ . This is accompanied in these cases by a sharp *increase* in the entanglement entropy. By increasing the length  $L_x$  of the system at fixed  $L_y$ , this final increase in the entanglement entropy can be pushed beyond the range of feasible calculations, and the simulation is guaranteed to obtain the MES. In the MES, the constant correction  $\gamma$  is entirely of topological origin, and is zero in discrete symmetry breaking states. Thus in this limit  $\gamma$  is the topological entanglement entropy, and a non-zero result proves that the state is a (topological) QSL. Moreover, we see from the above discussion that a positive  $\gamma$  can only come from topological order, so we do not obtain false positive signatures of topological order from symmetry breaking.

In Fig.5(a), we plot von Neumann entanglement entropy  $S(L_y)$  associated with the constant  $x$  cut which separates the cylinder into two symmetric parts of equal length,  $L_x/2$ , as a function of  $L_y$ , with  $L_y$  even (for  $L_y$  odd, there are additional effects which we discuss in Sec. V). By comparing systems of different lengths (Fig. 5b), we see that the entropy is essentially independent of  $L_x$  for  $L_x > 2L_y$ , and so equal to its

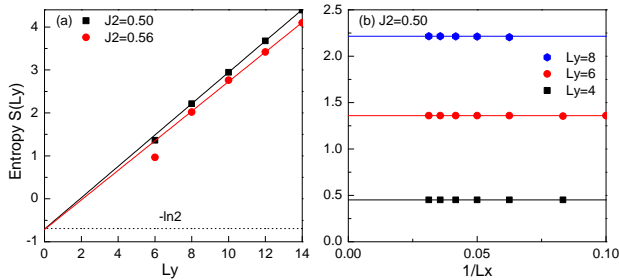


FIG. 5: (Color online) The entanglement entropy at  $J_2 = 0.5$  and  $0.56$ . (a) The entanglement entropy  $S(L_y)$  for  $L_y = 6 - 14$ . By fitting  $S(L_y) = aL_y - \gamma$ , we obtain  $\gamma \sim 0.70 \pm 0.02$  for  $J_2 = 0.5$ , and  $\gamma \sim 0.72 \pm 0.04$  for  $J_2 = 0.56$ . (b) Length dependence of the entanglement entropy for  $J_2 = 0.50$  and several system widths. One observes that the entropy is almost independent of  $L_x$  for long systems (a small increase with  $L_x$  can be observed for the smallest  $L_x$  at  $L_y = 8$ ).

limit at  $L_x = \infty$ . We then extrapolate  $\gamma$  from the fitting function  $S(L_y) = aL_y - \gamma$ . For  $J_2 = 0.5$ , deep in the magnetically disordered phase, our results show that  $\gamma = 0.70 \pm 0.02$ . This value appears constant, within numerical uncertainty, within the intermediate phase: for  $J_2 = 0.56$  (close to the quantum phase transition point  $J_2 = 0.62$ ), we obtain in the same way  $\gamma = 0.72 \pm 0.04$ . Without even consider the magnitude of  $\gamma$ , the fact that we see a negative rather than positive correction to the entanglement entropy is strong evidence against VBS order.

As mentioned in the Introduction, the topological entanglement entropy  $\gamma$  takes discrete values in topological phases. The minimum possible value for systems with unbroken time-reversal symmetry is  $\gamma = \ln(2) \approx 0.69$ , which is within 2% of the numerical results. The constancy of the numerical topological entanglement entropy and the consistency with the theoretically allowed value of  $\ln(2)$  constitute strong evidence for a topological QSL state. The appearance of the pure number  $\ln(2)$  (within happily small numerical uncertainty, of course) is certainly very striking coming out entirely unsolicited from the DMRG calculations.

Notably,  $\gamma = \ln(2)$  is the expected value for a  $Z_2$  QSL phase. The  $Z_2$  QSL is in many ways the simplest spin-liquid state, and has appeared repeatedly in theories of quantum magnets. As a rather complete theory of the low energy properties of  $Z_2$  QSLs is available, we can compare this to numerics in various ways.

## V. ODD-EVEN EFFECT

In this section, we make such a comparison based on the theory of the  $Z_2$  QSL. Specifically, in a  $Z_2$  QSL on the square lattice, it is predicted that cylinders with odd circumference – and not those with even circumference – should exhibit non-vanishing bulk staggered dimerization. This even-odd effect was first obtained, to our knowledge in Ref.38, by analysis of quantum dimer models<sup>39,40</sup>. Specifically, for a long cylinder

with (even)  $L_x \rightarrow \infty$  and odd  $L_y$ , the  $Z_2$  QSL induces a non-vanishing staggered dimerization,

$$\langle B_i^x \rangle = \overline{B^x} + D_x (-1)^{x_i}, \quad (3)$$

with  $D_x \sim e^{-L_y/\tilde{\xi}}$  exponentially decreasing with circumference. By contrast, no dimerization appears for even  $L_y$ . We obtain this behavior in Appendix A 1 directly from the effective  $Z_2$  gauge theory description, which shows that it is a *universal* feature of  $Z_2$  QSLs on the square lattice, and not particular to the quantum dimer models studied in Ref.<sup>38</sup>.

Precisely this behavior is observed in our numerics. Fig. 6(a,b) contrast the oscillatory and non-oscillatory horizontal bond expectation values obtained for odd and even  $L_y$ . For even  $L_y$ , some small boundary effects are observed, decaying over  $\sim 3$  lattice spacings. Fig.6(c) shows the exponential behavior of  $D_x$  obtained as the difference of even and odd bonds at the center of the sample. Interestingly, theories predict (see Ref.38 and also Supplementary Information)  $\tilde{\xi} = 2\xi$ , where  $\xi$  is the true dimer correlation length defined through the dimer correlation function. This explains the rather slow decay of  $D_x$ , which fits to  $\xi \approx 5$ , reasonably consistent with  $\xi_d \approx 4$  found (see Sec. II) from the examination of VBS correlation functions. While some even-odd effect might be expected in a columnar dimer phase for narrow cylinders, the exponentially-decaying behavior and results of other tests (see Sec. VI A) seem consistent only with a  $Z_2$  QSL.

## VI. DISCUSSION

The previous sections have shown that DMRG makes a compelling case for a non-magnetic intermediate state in the  $J_1$ - $J_2$  model. From direct measurements of the dimer order parameter and correlations, the intermediate state appears to have no or very weak VBS order. Most dramatically, we find a robust constant suppression of the entanglement entropy relative to the generic area law, known as *topological entanglement entropy*, which is a unequivocal signature of topological order. The value of the topological entanglement entropy we find is within 2% (and our numerical uncertainty) of the expected universal value  $\gamma = \ln(2)$  for the simplest  $Z_2$  QSL state, which suggests comparison of specific theoretical prediction for this  $Z_2$  phase to numerics. We indeed find a characteristic even-odd effect in the staggered dimerization, consistent with this state.

It is worth noting that ours is not the only suggestion of a QSL state in the  $J_1$ - $J_2$  model. Notably, after the initial version of this paper appeared, a parallel work<sup>41</sup> came to similar conclusions based on a tensor network variational method.

### A. Could this be a weak VBS state with strong finite size effects?

In our opinion the above results all point in the same direction, and are especially definitive given the seemingly unassailable implication of the observed topological entanglement

entropy. Nevertheless, following an earlier version of this paper, Sandvik<sup>32</sup> has suggested, by comparison with quantum Monte Carlo results for so-called J-Q models on cylinders, that similar behavior might occur for a system with a VBS ground state in the thermodynamic limit, due to strong finite size effects. We discuss this suggestion here.

### 1. Difference of models

The results of Ref. 32 are based on the J-Q models, which have four or six spin interactions (with coefficient  $Q$ ). These multi-spin interactions *explicitly* involve interactions between dimers, and as a consequence rather naturally favor VBS states. For instance, the simplest mean-field treatment of the Q term in the  $J$ - $Q_2$  model would proceed from by decoupling it by defining a mean-field dimer expectation value of the dimer operator, and thereby a VBS phase appears when the Q term becomes substantial. Thus it is natural and intuitive to expect a VBS phase in the J-Q models. By contrast, there is no a priori reason to expect dimer order in the  $J_1$ - $J_2$  model. The notion that a VBS state is somehow the most “likely” candidate for the intermediate non-magnetic state in the  $J_1$ - $J_2$  case is a misleading starting point. More importantly, we should be cautious in drawing conclusions from the J-Q models on the behavior of the  $J_1$ - $J_2$  model.

### 2. Entanglement entropy

The most direct evidence for a QSL state we have obtained is the topological entanglement entropy, remarkably close to the universal expected value for a  $Z_2$  QSL. In Ref. 32, Sandvik suggests that “it would not be surprising” if a system near a Néel to VBS transition (i.e. a DQCP) would exhibit a constant correction to the area law similar to that expected for a topological phase. In fact, we have shown theoretically that in a VBS state, there is indeed a constant correction *but of opposite sign* to that of a topological phase. Thus even forgetting the magnitude of  $\gamma$ , the sign alone is a strong argument against VBS order. The fact that the measured  $\gamma$  is within 2% of the very beautiful and universal expected result  $\ln(2)$  makes it hard to imagine this is mere coincidence.

In the context of a putative DQCP, the constant correction for a VBS state obtains if the system size is larger than the “deconfinement length”, below which there is an emergent U(1) symmetry unifying the plaquette and columnar VBS states, and linear combinations in between, with one another. Would one perhaps see a signal similar to the topological entanglement entropy were this length longer than the system size? Actually in this case we expect that the system should appear to exhibit a gapless Goldstone mode, characteristic of spontaneously breaking this U(1) symmetry. This is the situation discussed in Refs.35,36. In fact the behavior of the entanglement entropy in this case is even further from that of a topological phase: a *positive* logarithmic enhancement of the entanglement entropy beyond the area law is predicted, again of opposite sign to the topological case. Moreover, in

the 1d limit,  $L_x \gg L_y$ , the system should behave as a 1+1-dimensional conformal field theory with central charge  $c = 1$ , and hence exhibit a logarithmic growth of entanglement entropy,  $S(L) \sim \frac{1}{6} \ln(L_x)$ , in such a case. This is completely at odds with our observations – observe the constant behavior versus  $L_x$  in Fig. 5b.

### 3. VBS scaling

In Fig. 23 of Ref.32, our data for the dimerization is replotted along with data for the  $J$ - $Q_2$  model on a log-log plot, to fit to a single pure power law. Data for  $g(= J_2/J_1) = 0.5$  is compared to  $D_y^2 \sim L^{-\alpha}$  with  $\alpha \approx 1.8$ , and for  $g = 0.56$  is slightly above it. Small details of the data for the latter case for the smallest systems,  $L_x = 4, 6$ , are used to conclude that the system is VBS ordered in the infinite-size limit. We disagree. First, note the simple fact that the dimerization for the  $J_1$ - $J_2$  model is much smaller than that of the  $J$ - $Q_2$  model (which is the more weakly VBS ordered of the two J-Q models). Second, the scaling on this plot for the  $J_1$ - $J_2$  model (unlike the J-Q models) is quite close to  $\alpha = 2$ , which is, as mentioned in the same paragraph of Ref.32, exactly the behavior expected for a *non*-VBS phase.

### 4. Even-odd effects in VBS states

One of the pieces of evidence for the  $Z_2$  QSL state taken from our numerics was the very distinct behavior of the staggered dimerization in even and odd circumference systems, described in Sec. V. While this is certainly consistent with a  $Z_2$  state, one could imagine similar behavior arising in a system with VBS order in the thermodynamic limit. Here we consider the expected behavior in such a situation more carefully, for comparison to our results.

Consider a system which is spontaneously dimerized in the 2d limit, with a columnar dimer ground state. This state is four-fold degenerate, with four ground states consisting of two states with “horizontal dimers” staggered along the  $x$  direction ( $(\pi, 0)$  order), and two states with “vertical dimers” staggered along the  $y$  direction ( $(0, \pi)$  order). In the thermodynamic limit, these states are degenerate by rotation and translation symmetry. When confined to a cylinder, the anisotropy of the boundary conditions breaks the symmetry between the horizontal and vertical states. For the case of odd-width cylinders, the vertical dimerization is frustrated, because alternating “rows” of vertical dimers do not fit into the sample. This clearly would favor the horizontal dimer states. Amongst the two horizontal dimer states, the presence of an end to the system splits the remaining degeneracy, so all degeneracy is broken and we would expect long-range horizontal dimer order to appear. To this extent, the behavior for odd-width cylinders is the same as observed in our numerics, and as expected for the  $Z_2$  QSL. The difference is in the scaling. If the 2d system has a gapped dimer ground state, we would expect the expectation value of the dimerization to converge exponentially to a non-zero two dimensional limit as the width of the cylinder

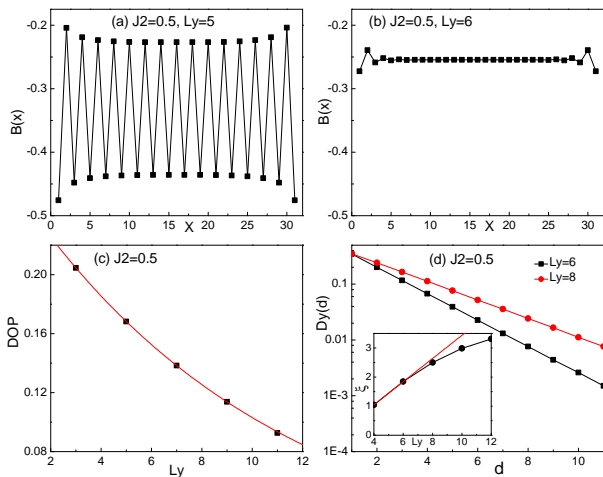


FIG. 6: (color online) Even-odd effect. (a) Expectation value of horizontal bond operator,  $\langle B_i^x \rangle$ , for  $L_y = 5$ ,  $L_x = 32$ . (b) The same expectation value for  $L_y = 6$ ,  $L_x = 32$ . (c) Dimer order parameter  $D_{d,\hat{x}}$  for odd  $L_y$  at  $L_x = \infty$ . The red line denotes the exponential-decaying fitting function with the form in Eq.(4). (d) Modified boundary induced dimer order parameter for  $L_y = 6, 8$ , with  $d$  the distance from the boundary. Here the dimer order parameter is defined as the dimer density difference between two nearest neighbor vertical dimer bonds. Inset shows the correlation length  $\xi$  along the cylinder as a function of  $L_y$ .

increases, i.e.

$$D_x|_{2d \text{ dimer state}} \sim \bar{D}_\infty + Ae^{-L_y/\tilde{\xi}}, \quad (4)$$

where  $A$  and  $\tilde{\xi}$  are constants, and  $\bar{D}_\infty$  is the value of the dimer order parameter in the thermodynamic limit.

As shown in Fig.6(c), the numerical fitting to this form gives  $\bar{D}_\infty = 0$  within numerical accuracy. This is entirely consistent with vanishing VBS order and a  $Z_2$  QSL in the thermodynamic limit, but of course cannot exclude some weak dimerization smaller than our numerical uncertainties. It seems to us natural to take the former interpretation, since it is simpler. According to the theory for the  $Z_2$  QSL discussed in Appendix A 1 and quantum dimer model results<sup>38</sup>, an exponential decay for the staggered dimerization is expected with “doubled” correlation length  $\tilde{\xi} = 2\xi$ , where  $\xi$  is the true VBS correlation length. We find  $\tilde{\xi} \approx 10$  lattice spacings, which is equivalent via Eq. (A28) to  $\xi \approx 5$ .

For the even circumference cylinders, the vertical dimer order is unfrustrated, and it is an energetic question, which likely depends upon the details of the model, whether the vertical or horizontal dimer order would be favored in this case. If the horizontal dimer state is favored, then we again expect behavior like Eq. (4), which is manifestly inconsistent with our numerics, and markedly different from the  $Z_2$  QSL. However, it is perfectly conceivable that the vertical dimer pattern is favored instead. If so, the periodic boundary conditions do not break the symmetry between the two vertical dimer states, and so we expect the DMRG to converge to the symmetric linear combination of the two dimer states, which lacks any spontaneous dimer pattern. So at least the presence of an even-odd

effect in the static dimerization is consistent with a VBS state, if the cylindrical geometry favors the two VBS states with horizontal rows of vertical dimers. On the face of it, this appears consistent with our numerical results *for the staggered dimerization*, if one assumes that the value of the dimerization itself (extrapolated from odd circumference cylinders) is smaller than our numerical uncertainty. But it is worth pointing out that for this scenario to hold, the even circumference system must be in a Schrödinger cat state, and should exhibit a positive  $\ln(2)$  enhancement of the entanglement entropy (negative TEE) as a consequence, and moreover convergence to such a state should be progressively more difficult with increasing  $L_x$ . This is not at all what we see.

## 5. End effects

In Ref. 32, strong boundary effects are observed on the dimerization in the J-Q models. Indeed, on symmetry grounds, an open end breaks translation and reflection symmetries in the  $x$  direction, and as such should act as a “boundary field” on the staggered dimer order  $D_x$ , i.e. it induces a term  $-\lambda D_x(x=0)$  in a Landau theory of this order. On these grounds, we always expect some staggered dimer order near the boundary. If it is energetically disfavored in the bulk, this will decay rapidly. Otherwise, it will penetrate deep into the bulk. In the J-Q models, it was found that the boundaries induce a quite strong dimerization, so that *for even*  $L_y$  the bond expectation values  $\langle B_i^x \rangle$  oscillate visibly (c.f. in the inset of Fig. 6, and in Fig. 15a of Ref.32, the bond expectation value shows oscillations with large amplitude in the J-Q<sub>3</sub> and J-Q<sub>2</sub> models, respectively). By contrast, in the  $J_1$ - $J_2$  model, we see in Fig. 6(b) that there are no visible oscillations in the same quantity when  $L_y$  is even. This qualitative difference tells us that  $D_x$  order is clearly much less favorable in the  $J_1$ - $J_2$  model.

We next try to address the possibility, raised above, that the cylindrical geometry when  $L_y$  is even favors  $D_y$  order, i.e. horizontal rows of vertical dimers. This is at odds with our measurements of the dimer correlations and the entanglement entropy. Still, it is more compelling to explicitly test to rule out the possibility directly. To do so, we have studied several modified cylinders with even circumference, in which the ends of the cylinder have been altered, breaking translational symmetry along  $y$  in order to break the degeneracy and favor one of the two vertical dimer states. What we observe is that in all cases, as shown in Fig.6(d), although dimer order is induced by this symmetry breaking in the vicinity of the boundary, it decays exponentially into the bulk of the cylinder. The correlation length  $\xi_v$  for this vertical dimer order still depends on circumference for the system sizes in our study, so we plot it versus  $L_y$  to see if it is limited by the system size (it does not appear to be), and to extrapolate from this its value in the thermodynamic limit. We observe that this correlation length grows sub-linearly in  $L_y$ , and extrapolates to  $\xi_v \sim 4$  in the 2D limit (i.e.,  $L_y = \infty$ ). This is very different from what would be expected for a 2d state with long-range dimer order, in which the non-zero stiffness (surface tension) of the

ordered dimer state would prevent such decay (we would expect  $\xi_v = \infty$  in this case). If one were to imagine that the system were proximate to a DQCP, and  $L_y$  were smaller than the deconfinement length, then we would instead expect  $\xi_v \propto L_y$ , which again is not consistent with our results. Note also that the value for  $\xi_v$  is quite consistent with the value for  $\tilde{\xi}$  obtained earlier. The fact that vertical dimer order decays away, even when the most favorable conditions have been created for it, is strong evidence against VBS order in the 2d limit.

## B. Summary and Open Issues

In conclusion, we have presented compelling evidence from accurate DMRG calculations for a topological QSL state in the two dimensional  $J_1$ - $J_2$  Heisenberg model. This is the simplest example of such a QSL discovered to date, and the only one to our knowledge for a Heisenberg model on a Bravais lattice. As such, it is particularly attractive for further theoretical and experimental study. We anticipate, for instance, that our discovery will afford an opportunity to explore the QSL mechanism of unconventional superconductivity<sup>4,42</sup> in a controlled theoretical setting.

Another consequence of topological order is the presence of quasi-degenerate ground states on the torus or cylinder. A two-fold quasi-degeneracy is expected for a  $Z_2$  QSL on the cylinder studied here, with a splitting of order  $L_x e^{-L_y/\xi}$  in the case of long cylinders, where  $\xi$  is the spin-spin correlation length (see Appendix A 2). As shown in Ref.37 and discussed in Sec. IV, the DMRG preferentially converges, however, to just *one* of the quasi-degenerate ground states (specifically, a minimally entangled state). This explains the absence of an observed topological degeneracy in this and other DMRG studies.<sup>7,37,43</sup> It is a non-trivial and open problem to obtain the second ground state and thereby extract the topological energy splitting. It is our expectation that it is actually orders

of magnitude smaller than the bulk energy gaps.

The nature of the quantum phase transitions from the QSL to Néel and striped antiferromagnetic phases is an interesting topic for future study. Though we have not focused on the transitions themselves, and more work is clearly required to make strong conclusions about them numerically, it appears that the transition from the Néel to QSL state may be continuous. Ref.32 erroneously claims that a Néel to QSL transition might be in the same universality class as the DQCP between Néel and VBS order, because “the operator causing the VBS order is dangerously invariant”. Though at the DQCP the operator which *distinguishes* between columnar and plaquette VBS order is dangerously *irrelevant*, even when this operator’s coefficient in the Hamiltonian is tuned to zero, the non-magnetic phase has spontaneous VBS order. So this claim is incorrect. In fact, such a transition requires an entirely different theory. A novel suggestion for the theory of this critical point has been made in Ref.44, and it would be interesting to compare it to further numerical studies.

## Acknowledgments

We would like to thank Cenke Xu, Ashvin Vishwanath, Zheng-Yu Weng, Steve White, Zhenyue Zhu, Max A. Metlitski, Dong-Ning Sheng, Zheng-Cheng Gu and H.Y. especially thanks Steve Kivelson for inspiring discussions. This work was supported in part by the NBRPC (973 Program) 2011CBA00300 (2011CBA00302). H.C.J. sincerely thanks the hospitality of Microsoft Station Q, where part of the numerical simulation was done on the Cirrus cluster. H.Y. was supported by NSF Grant DMR-0904264 at Stanford. L.B. and H.C.J. were supported by NSF grant DMR-0804564. This work was partially supported by the the KITP NSF grant PHY05-51164 and the NSF MRSEC Program under Award No. DMR 1121053.

- 
- <sup>1</sup> L. Balents, Nature **464**, 199 (2010).  
<sup>2</sup> X. G. Wen, Phys. Rev. B **40**, 7387 (1989).  
<sup>3</sup> X. Wen, Int. J. Mod. Phys. B **4**, 239 (1990).  
<sup>4</sup> S. A. Kivelson, D. S. Rokhsar, and J. P. Sethna, Phys. Rev. B **35**, 8865 (1987).  
<sup>5</sup> P. W. Anderson, Materials Research Bulletin **8**, 153 (1973).  
<sup>6</sup> Z. Meng, T. Lang, S. Wessel, F. Assaad, and A. Muramatsu, Nature **464**, 847 (2010).  
<sup>7</sup> S. Yan, D. Huse, and S. White, Science **332**, 1173 (2011).  
<sup>8</sup> K. Seo, B. A. Bernevig, and J. Hu, Phys. Rev. Lett. **101**, 206404 (2008).  
<sup>9</sup> Q. Si and E. Abrahams, Phys. Rev. Lett. **101**, 076401 (2008).  
<sup>10</sup> C. Fang, H. Yao, W.-F. Tsai, J. Hu, and S. A. Kivelson, Phys. Rev. B **77**, 224509 (2008).  
<sup>11</sup> C. Xu, M. Müller, and S. Sachdev, Phys. Rev. B **78**, 020501 (2008).  
<sup>12</sup> H. C. Jiang, F. Krüger, J. E. Moore, D. N. Sheng, J. Zaanen, and Z. Y. Weng, Phys. Rev. B **79**, 174409 (2009).  
<sup>13</sup> R. Melzi, S. Aldrovandi, F. Tedoldi, P. Carretta, P. Millet, and F. Mila, Phys. Rev. B **64**, 024409 (2001).  
<sup>14</sup> V. N. Kotov, J. Oitmaa, O. P. Sushkov, and Z. Weihong, Phys. Rev. B **60**, 14613 (1999).  
<sup>15</sup> E. Dagotto and A. Moreo, Phys. Rev. Lett. **63**, 2148 (1989).  
<sup>16</sup> L. Capriotti and S. Sorella, Phys. Rev. Lett. **84**, 3173 (2000).  
<sup>17</sup> M. Mambrini, A. Läuchli, D. Poilblanc, and F. Mila, Phys. Rev. B **74**, 144422 (2006).  
<sup>18</sup> X. G. Wen, Phys. Rev. B **44**, 2664 (1991).  
<sup>19</sup> F. Figueirido, A. Karlhede, S. Kivelson, S. Sondhi, M. Rocek, and D. S. Rokhsar, Phys. Rev. B **41**, 4619 (1990).  
<sup>20</sup> M. P. Gelfand, R. R. P. Singh, and D. A. Huse, Phys. Rev. B **40**, 10801 (1989).  
<sup>21</sup> N. Read and S. Sachdev, Phys. Rev. Lett. **62**, 1694 (1989).  
<sup>22</sup> P. Chandra, P. Coleman, and A. Larkin, Journal of Physics: Condensed Matter **2**, 7933 (1990).  
<sup>23</sup> M. E. Zhitomirsky and K. Ueda, Phys. Rev. B **54**, 9007 (1996).  
<sup>24</sup> R. Darradi, O. Derzhko, R. Zinke, J. Schulenburg, S. E. Krüger, and J. Richter, Phys. Rev. B **78**, 214415 (2008).  
<sup>25</sup> J. Richter and J. Schulenburg, The European Physical Journal B-Condensed Matter and Complex Systems **73**, 117 (2010).  
<sup>26</sup> A. Kitaev and J. Preskill, Phys. Rev. Lett. **96**, 110404 (2006).

- <sup>27</sup> M. Levin and X.-G. Wen, Phys. Rev. Lett. **96**, 110405 (2006).  
<sup>28</sup> T. Senthil, A. Vishwanath, L. Balents, S. Sachdev, and M. Fisher, Science **303**, 1490 (2004).  
<sup>29</sup> S. R. White, Phys. Rev. Lett. **69**, 2863 (1992).  
<sup>30</sup> S. R. White and A. L. Chernyshev, Phys. Rev. Lett. **99**, 127004 (2007).  
<sup>31</sup> E. M. Stoudenmire and S. R. White, arXiv:1105.1374 (2011).  
<sup>32</sup> A. W. Sandvik, Phys. Rev. B **85**, 134407 (2012).  
<sup>33</sup> A. W. Sandvik, Phys. Rev. B **56**, 11678 (1997).  
<sup>34</sup> V. Murg, F. Verstraete, and J. I. Cirac, Phys. Rev. B **79**, 195119 (2009).  
<sup>35</sup> M. A. Metlitski and T. Grover, ArXiv e-prints (2011), 1112.5166.  
<sup>36</sup> A. B. Kallin, M. B. Hastings, R. G. Melko, and R. R. P. Singh, Phys. Rev. B **84**, 165134 (2011).  
<sup>37</sup> H.-C. Jiang, Z. Wang, and L. Balents ArXiv e-prints (2012), 1205.4289.  
<sup>38</sup> H. Yao and S. A. Kivelson, arXiv:1112.1702 (Phys. Rev. Lett. in press) (2011).  
<sup>39</sup> D. S. Rokhsar and S. A. Kivelson, Phys. Rev. Lett. **61**, 2376 (1988).  
<sup>40</sup> R. Moessner and S. L. Sondhi, Phys. Rev. Lett. **86**, 1881 (2001).  
<sup>41</sup> L. Wang, Z. C. Gu, F. Verstraete, and X. G. Wen, ArXiv e-prints (2011), 1112.3331.  
<sup>42</sup> P. W. Anderson, Science **235**, 1196 (1987).  
<sup>43</sup> H. C. Jiang, Z. Y. Weng, and D. N. Sheng, Phys. Rev. Lett. **101**, 117203 (2008).  
<sup>44</sup> E.-G. Moon and C. Xu, ArXiv e-prints (2012), 1204.5486.  
<sup>45</sup> T. Senthil and M. Fisher, Physical Review B **62**, 7850 (2000).  
<sup>46</sup> D. Blankschtein, M. Ma, and A. N. Berker, Phys. Rev. B **30**, 1362 (1984).  
<sup>47</sup> C. Xu and L. Balents, Phys. Rev. B **84**, 014402 (2011).  
<sup>48</sup> T. Senthil and M. P. A. Fisher, Phys. Rev. B **63**, 134521 (2001).  
<sup>49</sup> Y. Zhang, T. Grover, A. Turner, M. Oshikawa, and A. Vishwanath, ArXiv e-prints (2011), 1111.2342.

### Appendix A: $Z_2$ gauge theory

Here we discuss an effective  $Z_2$  gauge theory description of the QSL state,<sup>45</sup> and in particular derive the behavior of the dimerization and ground state quasi-degeneracy discussed in the main text. We begin with the Hamiltonian

$$H = -K \sum_{\square} \prod_{\langle ij \rangle \in \square} \sigma_{ij}^z - h \sum_{\langle ij \rangle} \sigma_{ij}^x + r \sum_i n_i \quad (\text{A1})$$

$$- \sum_{\langle ij \rangle} \sigma_{ij}^z \left[ t b_{i\alpha}^\dagger b_{j\alpha} + \Delta \eta_i (b_{i\alpha} \epsilon_{\alpha\beta} b_{j\alpha} + \text{h.c.}) \right],$$

where  $n_i = b_{i\alpha}^\dagger b_{i\alpha}$  and  $\eta_i = (-1)^{x_i+y_i}$ . We introduced ‘‘spinon’’ operators  $b_{i\alpha}$  which transform as spinors under  $SU(2)$ , and obey standard commutation relations  $[b_{i\alpha}, b_{j\beta}^\dagger] = \delta_{ij} \delta_{\alpha\beta}$ . The physical spin operators are related to them by  $\mathbf{S}_i = \frac{1}{2} b_{i\alpha}^\dagger \boldsymbol{\sigma}_{\alpha\beta} b_{i\beta}$ . The  $\sigma_{ij}^z$  operators are Pauli matrix  $Z_2$  gauge fields, which we will refer to as the ‘‘magnetic’’ gauge fields.  $Z_2$  gauge symmetry is enforced by the constraint

$$\prod_{|j-i|=1} \sigma_{ij}^x = -(-1)^{n_i}. \quad (\text{A2})$$

Note that the product in Eq. (A2) is over  $j$  not  $i$ . This is the analog of Gauss’ law for the ‘‘electric’’ field  $\sigma_{ij}^x$ . This constraint ‘‘generates’’ the Ising gauge symmetry  $\sigma_{ij}^z \rightarrow s_i s_j \sigma_{ij}^z$ ,

$b_i \rightarrow s_i b_i$ , where  $s_i = \pm 1$  can be chosen arbitrarily for each site.

### 1. Staggered dimerization

Here we obtain the behavior of the staggered dimerization from the  $Z_2$  gauge theory. For this purpose, it is sufficient to integrate out the spinons, since we discuss local properties of the QSL state which has a spin gap (but see below Sec. A 2). We can obtain this limit from Eq. (A1) by taking  $r$  large, which projects the problem onto the subspace with  $n_i = 0$ . Then the Hamiltonian reduces to

$$H = -K \sum_{\square} \prod_{\langle ij \rangle \in \square} \sigma_{ij}^z - h \sum_{\langle ij \rangle} \sigma_{ij}^x, \quad (\text{A3})$$

and

$$\prod_{|j-i|=1} \sigma_{ij}^x = -1. \quad (\text{A4})$$

Eqs. (A3,A4) describe the ‘‘odd Ising gauge theory’’. It is in the deconfined (QSL) phase for  $K/h > x_c$ , where  $x_c$  is some order one number specifying the critical point.

Now consider the staggered dimerization,  $D_x = (-1)^{x_i} \langle D_i^x \rangle - \langle D_{i+\hat{x}}^x \rangle$ , defined in the main text. On symmetry grounds, we expect that  $\langle D_i^x \rangle \propto \langle \sigma_{i,i+\hat{x}}^x \rangle$  (this relation can also be derived by perturbation theory in  $t/r$ ). We will derive the odd/even effect for the staggered dimerization in finite-width cylinders in two ways. First, we obtain it directly from the Ising gauge theory in the strong coupling limit, which is a very short derivation. Second, we obtain it using duality and field theory, which exposes the universal nature of the staggered dimerization and its relation to  $Z_2$  vortex (‘‘vison’’) excitations.

To see how one might expect the dimerization, we first consider the ‘‘topological’’ operator

$$Q_x = \prod_{y=1}^{L_y} \sigma_{xy;x+1y}^x. \quad (\text{A5})$$

This operator commutes with  $H$  and is thus a constant of the motion. Moreover, if we consider the case  $x = 1$  at the left hand side of the system, we obtain

$$Q_1 = \prod_{y=1}^{L_y} \left( \prod_{|j-i|=1} \sigma_{ij}^x \right)_{i=(1,y)} = (-1)^{L_y}, \quad (\text{A6})$$

where we have used Eq. (A4). Again using Eq. (A4), one obtains

$$Q_x = (-1)^{x L_y}. \quad (\text{A7})$$

Thus  $Q_x = 1$  for even  $L_y$ , but oscillates,  $Q_x = (-1)^x$ , for odd  $L_y$ . Although this is not the dimerization itself, it suggests the presence of staggered dimerization in the case of odd  $L_y$ .

a. *Direct derivation*

We now turn to the first derivation, working deep in the deconfined phase, taking  $K \gg h$ , and proceed by direct calculation perturbatively in  $h$ . For  $h = 0$ , the ground state(s) are obtained by simply choosing a classical configuration of  $\sigma_{ij}^z$  with zero Ising gauge flux,  $\prod_{\langle ij \rangle \in \square} \sigma_{ij}^z = 1$  on all plaquettes (for instance the state with  $\sigma_{ij}^z = +1$  on all bonds), and then projecting this state to satisfy Eq. (A4):

$$|\psi_0\rangle = \prod_i \hat{P}_i |\sigma_{ij}^z = 1\rangle, \quad (\text{A8})$$

where

$$\hat{P}_i = \frac{1}{2} - \frac{1}{2} \prod_{|j-i|=1} \sigma_{ij}^x \quad (\text{A9})$$

In this state, the expectation value of  $\sigma_{ij}^x$  vanishes. This can be seen as follows. Define the Wilson loop operator

$$W[\mathcal{C}] = \prod_{\langle ij \rangle \in \mathcal{C}} \sigma_{ij}^z, \quad (\text{A10})$$

where  $\mathcal{C}$  is a closed curve on the lattice. All such Wilson loops commute with the projectors  $\hat{P}_i$ , so  $|\psi_0\rangle$  is an eigenstate of the Wilson loop with  $W[\mathcal{C}]|\psi_0\rangle = |\psi_0\rangle$ . Moreover, since  $W[\mathcal{C}]^2 = 1$ , we have

$$\langle \psi_0 | \sigma_{ij}^x | \psi_0 \rangle = \langle \psi_0 | W[\mathcal{C}] \sigma_{ij}^x W[\mathcal{C}] | \psi_0 \rangle = -\langle \psi_0 | \sigma_{ij}^x | \psi_0 \rangle = 0, \quad (\text{A11})$$

if we choose  $\mathcal{C}$  to be a curve containing the both  $\langle ij \rangle$ . To achieve a non-zero result, we must consider non-zero orders of perturbation theory in  $h/K$ . In general, the form of the perturbative eigenstate is

$$|\psi\rangle \propto \sum_{n=0}^{\infty} c_n \left[ \hat{R} H' \right]^n |\psi_0\rangle, \quad (\text{A12})$$

where  $\hat{R} = P(E_0 - H_0)^{-1}P$  is the resolvent with  $H_0 = H(h = 0)$  and  $E_0$  the ground state energy of  $H_0$  and  $P = 1 - |\psi_0\rangle\langle\psi_0|$  is the projector onto the unperturbed excited state subspace,  $H' = H - H_0 = -h \sum_{\langle ij \rangle} \sigma_{ij}^x$ , and the  $c_n$  are numerical coefficients. This can be expanded to give a series of terms, each involving a product of  $n$  electric gauge fields acting on  $|\psi_0\rangle$  at  $O[(h/K)^n]$ . For each such term, we can repeat the argument in Eq. (A11). We will achieve a vanishing result provided we can choose  $\mathcal{C}$  to contain an odd number of links that coincide with the set of links  $\mathcal{L}$  containing the electric fields in the corresponding term in the wavefunction and the link  $\langle ij \rangle$  in the expectation value. This is always possible unless the ‘‘dual’’ of  $\mathcal{L}$  forms a closed loop. This dual is formed by associating a link of the dual lattice with each link in  $\mathcal{L}$ . If the dual of  $\mathcal{L}$  indeed forms a closed loop, then the closed loop  $\mathcal{C}$  must intersect it an even number of times.

Thus we obtain non-zero contributions only from terms in which  $\mathcal{L}$  is comprised of closed dual loops. There are trivial contributions from short loops, the minimal one being the

case when  $\mathcal{L}$  contains  $\langle ij \rangle$  twice, which is first order in  $h/K$ . This gives a non-zero constant contribution to the expectation value, but one which is *uniform*, and hence does not correspond to a staggered dimerization. A non-trivial result is obtained first at  $O[(h/K)^{L_y-1}]$ , from the smallest closed dual loop encircling the cylinder and containing the bond due to  $\langle ij \rangle$ , which must be a horizontal bond. This leading term arises from the  $O[(h/K)^m]$  correction to the ground state ket and the  $O[(h/K)^{L_y-1-m}]$  correction to the ground state bra ( $m = 0, 1, \dots, L_y - 1$ ), giving

$$\begin{aligned} \langle \sigma_{ii+\hat{x}}^x \rangle &= \quad (\text{A13}) \\ \dots + C_n \sum_{m=0}^{L_y-1} \binom{L_y-1}{m} \left(\frac{h}{K}\right)^{(L_y-1)} \langle \psi_0 | Q_{x_i} | \psi_0 \rangle \\ &= \dots + C_n \left(\frac{2h}{K}\right)^{L_y-1} (-1)^{L_y x}. \end{aligned}$$

Here  $C_n$  is a numerical coefficient which should be determined from a more refined analysis. We therefore conclude that for odd  $L_y$ , we obtain the staggered dimerization discussed in the main text, with amplitude  $D_x \sim (2h/K)^{L_y-1} = \exp[-\ln(K/2h)(L_y - 1)]$ , exponentially decaying with circumference as advertised. This result derived from the odd Ising gauge theory is qualitatively consistent with the one obtained from the analysis<sup>38</sup> of quantum dimer models.

b. *Dual derivation*

While the above derivation is simple and direct, it relies on the strong coupling expansion, which, although it is expected to be qualitatively correct in the deconfined phase, is not obviously general. It is instructive to obtain the staggered dimerization by a more circuitous dual route, which exposes the universality of the result and gives a more direct physical picture.

The duality transformation of Eqs. (A3,A4) is accomplished by defining

$$\tau_a^x = \prod_{\langle ij \rangle \in a} \sigma_{ij}^z, \quad (\text{A14})$$

$$\sigma_{ij}^x = \mu_{ab} \tau_a^z \tau_b^z, \quad (\text{A15})$$

where  $\tau_a$  are new Pauli matrices. In Eq. (A14)  $\langle ij \rangle$  are the bonds associated with dual site  $a$  at the center of a direct plaquette, and in Eq. (A15), the dual sites  $a, b$  are those at the centers of the two plaquettes neighboring the bond  $\langle ij \rangle$ . The scalars  $\mu_{ab}$  must be chosen to satisfy Eq. (A4), which requires that their product around a dual plaquette must equal  $-1$ . The dual Hamiltonian is then a fully frustrated transverse field Ising model:

$$H = -h \sum_{\langle ab \rangle} \mu_{ab} \tau_a^z \tau_b^z - K \sum_a \tau_a^x. \quad (\text{A16})$$

The  $\tau_a^z$  operator has the physical interpretation of creating an Ising vortex (vison) on plaquette  $a$ . In the deconfined phase,

when  $K/h > x_c$ , the visons are gapped excitations in the “paramagnetic” phase of this dual Ising model. We will see that the dimerization is related to virtual vison excitations.

To see this, we obtain a continuum limit of Eq. (A16), valid in the deconfined phase, as follows (qualitatively identical results can be obtained in many other ways, for instance by an expansion about mean field theory, or by strong coupling expansions). It is convenient to work in a path integral formulation in the  $\tau_a^z$  basis, and “soften” the spins  $\tau_a^z \rightarrow \varphi_a$ . The Euclidean action in the time continuum limit is then

$$S = \int d\tau \left\{ -h \sum_{\langle ab \rangle} \mu_{ab} \varphi_a \varphi_b + \sum_a \left[ \frac{\kappa}{2} (\partial_\tau \varphi_a)^2 + \frac{r}{2} \varphi_a^2 + u \varphi_a^4 \right] \right\}, \quad (\text{A17})$$

where  $\kappa, r$  and  $u$  are phenomenological parameters. In the deconfined phase, the fluctuations of  $\varphi_a$  are small, and it is sufficient to truncate the action to quadratic order. The dominant fluctuations are those near the minimum of the quadratic form. To find them, we must choose a gauge for the frustrated dual exchange. It is convenient to make the following choice:

$$\mu_{a,a+\hat{y}} = (-1)^{x_a}, \quad \mu_{a,a+\hat{x}} = 1. \quad (\text{A18})$$

Here we have taken the dual lattice sites to have integer coordinates. The unit cell in this gauge contains two sites. Therefore, Fourier transforming to go to the Bloch basis, we obtain the inverse Green’s function describing the virtual fluctuations of the visons,

$$G^{-1} = (\kappa \omega_n^2 + r)I - 4h \begin{pmatrix} \cos k_y & \cos k_x \\ \cos k_x & -\cos k_y \end{pmatrix}. \quad (\text{A19})$$

Here the “magnetic” Brillouin zone is  $|k_x| \leq \pi/2, |k_y| \leq \pi$ . The dominant fluctuations, corresponding to the minimum eigenvalue of  $G^{-1}$  ( $= r - 4\sqrt{2}h$ ), occur at the two inequivalent values  $(k_x, k_y) = (0, 0)$  and  $(k_x, k_y) = (0, \pi)$ . The corresponding eigenvectors are  $\phi^{(1)} = (\cos \frac{\pi}{8}, \sin \frac{\pi}{8})$  at  $k = (0, 0)$  and  $\phi^{(2)} = (\sin \frac{\pi}{8}, \cos \frac{\pi}{8})$  at  $k = (0, \pi)$ . Focusing on these lowest energy excitations, we therefore write

$$\varphi_a \sim \phi_a^{(1)} \Phi_1(x_a, y_a) + \phi_a^{(2)} (-1)^{y_a} \Phi_2(x_a, y_a), \quad (\text{A20})$$

where  $\phi_a^{(i)}$  takes the two values of eigenvector  $i$  given above when  $a$  is on the two distinct sublattices, and  $\Phi_i(x, y)$  is a slowly-varying continuum field. The bulk effective action is then

$$S = \frac{\kappa}{2} \sum_{i=1,2} \int d\tau dx dy \left\{ (\partial_\tau \Phi_i)^2 + v^2 (\nabla \Phi_i)^2 + m^2 \Phi_i^2 \right\} \quad (\text{A21})$$

This action describes two degenerate minimum energy vison states. It was discussed first to our knowledge in Ref.<sup>46</sup>, in the context of frustrated Ising models. It is instructive to express the VBS order parameter in terms of  $\Phi_i$ . If we consider the

horizontal bonds,

$$\begin{aligned} D_x &= (-1)^{x_i} (\mathbf{S}_i \cdot \mathbf{S}_{i+\hat{x}} - \mathbf{S}_{i+\hat{x}} \cdot \mathbf{S}_{i+2\hat{x}}) \\ &\sim (-1)^{x_i} (\sigma_{i,i+\hat{x}}^x - \sigma_{i+\hat{x},i+2\hat{x}}^x) \\ &\sim (-1)^{x_i} (\tau_a^z \tau_{a+\hat{y}}^z + \tau_{a+\hat{x}}^z \tau_{a+\hat{x}+\hat{y}}^z) \\ &\sim (c\Phi_1 + s\Phi_2)(c\Phi_1 - s\Phi_2) - (s\Phi_1 + c\Phi_2)(s\Phi_1 - c\Phi_2) \\ &\sim \Phi_1^2 - \Phi_2^2, \end{aligned} \quad (\text{A22})$$

where in the penultimate line of Eq. (A22),  $c = \cos \pi/8$  and  $s = \sin \pi/8$ . By a similar calculation, one finds that the vertical bond dimerization is

$$D_y = (-1)^{y_i} (\mathbf{S}_i \cdot \mathbf{S}_{i+\hat{y}} - \mathbf{S}_{i+\hat{y}} \cdot \mathbf{S}_{i+2\hat{y}}) \sim 2\Phi_1\Phi_2. \quad (\text{A23})$$

From this we obtain the result

$$\Psi = D_x + iD_y \sim (\Phi_1 + i\Phi_2)^2. \quad (\text{A24})$$

The gauge invariant combination on the right hand side can thus be identified as the familiar complex VBS order parameter  $\Psi$ . This result, and the action Eq. (A21), have been obtained many times for quantum spin-1/2 systems on the square lattice. Indeed, both are largely independent of the microscopic model, and give the *minimal* set of excitations and their properties gives only the assumptions of  $Z_2$  topological order in the ground state and half-integer spin per unit cell. It would be interesting to understand if other dimer patterns could in principle arise, if the low energy vison states were selected from a different projective symmetry group.<sup>47</sup> In two dimensions, in the  $Z_2$  QSL phase, there is no VBS order, so the visons are gapped and the VBS order parameter  $\Psi$  also is uncondensed, correspondingly.

We now consider the finite-size effects. Taking periodic boundary conditions on  $\varphi_a$  in the  $y$  direction imposes, using Eq. (A20), periodic boundary conditions on  $\Phi_1$  but *anti-periodic* boundary conditions on  $\Phi_2$  when  $L_y$  is odd. The latter result can be readily understood in terms of the VBS order parameter: on an odd-leg cylinder, the vertical component  $D_y$  is frustrated (staggering of rows of dimers does not “fit”) and should be antiperiodic, which requires  $\Psi \rightarrow \Psi^*$  under the circuit around the cylinder, consistent with the anti-periodic boundary conditions on  $\Phi_2$ . Since the visons are gapped, the antiperiodic boundary condition gives an exponentially small effect in the thermodynamic limit, but it is non-zero and can be readily calculated.

Regardless of boundary conditions, because  $\Phi_1$  and  $\Phi_2$  are decoupled in Eq. (A21),  $\langle D_y \rangle = 0$ , so there is no VBS order of the vertical bonds. The horizontal component, however, is non-zero when  $L_y$  is odd, so that the fields  $\Phi_1$  and  $\Phi_2$  are slightly inequivalent due to the boundary conditions:

$$\begin{aligned} \langle D_x \rangle &\sim \langle \Phi_1^2 \rangle - \langle \Phi_2^2 \rangle \\ &\sim \kappa^{-1} \int \frac{d\omega_n}{2\pi} \frac{dk_x}{2\pi} \left[ \frac{1}{L_y} \sum_{k_y} \frac{1}{\omega_n^2 + v^2 k^2 + m^2} \right. \\ &\quad \left. - \frac{1}{L_y} \sum_{k_y} \frac{1}{\omega_n^2 + v^2 k^2 + m^2} \right], \end{aligned} \quad (\text{A25})$$

where the first sum is over ‘‘periodic’’ momenta  $k_y = 2\pi n/L_y$ , and the second sum (with the prime) is over ‘‘anti-periodic’’ momenta  $k_y = 2\pi(n + 1/2)/L_y$ , with integer  $n$ . To proceed, we first perform the frequency integration and then use the Poisson resummation formula to obtain

$$\begin{aligned} \langle D_x \rangle &\sim \frac{2}{\kappa} \sum_{p=0}^{\infty} \int \frac{dk_x}{2\pi} \int \frac{dk_y}{2\pi} \frac{\cos[(2p+1)k_y L_y]}{\sqrt{v^2 k^2 + m^2}} \quad (\text{A26}) \\ &\sim \frac{2}{\pi \kappa v} \sum_{p=0}^{\infty} \int \frac{dk_x}{2\pi} M(k_x) K_0[(2p+1)M(k_x)L_y/v], \end{aligned}$$

where we carried out the  $k_y$  integration in the last line, and defined  $M(k_x) = \sqrt{m^2 + v^2 k_x^2}$ . For large  $L_y$ , the asymptotic form of the Bessel function can be used,  $K_0(z) \sim \sqrt{\pi/2z} e^{-z}$ , and the dimerization is dominated by the  $p = 0$  term and the region  $vk_x \ll m$ :

$$\begin{aligned} \langle D_x \rangle &\sim \frac{2}{\pi \kappa v} \sqrt{\frac{\pi v}{m L_y}} \int \frac{dk_x}{2\pi} m e^{-m L_y/v} e^{-v k_x^2 L_y/2m} \\ &\sim \frac{\sqrt{2}m}{\pi \kappa v L_y} e^{-m L_y/v}. \quad (\text{A27}) \end{aligned}$$

As promised, we obtain exponential decay of the dimerization, and in this case a prediction for the prefactor. The physics of this derivation is transparent: virtual fluctuations of  $Z_2$  vortices which propagate about the cylinder lead directly to the dimerization. In this way we immediately see that this effect is universal for  $Z_2$  QSLs on the square lattice with  $S = 1/2$  spins.

Let us conclude this subsection with one remark on the dimer correlation lengths. The static dimerization on cylinders with odd circumference decays with an apparent correlation length  $\tilde{\xi} = v/m$ . This is *not* the same length which appears in the dimer-dimer correlation function. The latter is obtained from correlation functions of  $\Psi$ , given in Eq. (A24). Because the dimer order parameter  $\Psi$  is quadratic in the vison fields  $\Phi_i$ , and the  $\Phi_i$  are Gaussian distributed, by Wick’s theorem the dimer-dimer correlation functions are *squares* of vison Green’s functions. Consequently, the exponential decay of the dimer-dimer correlation function, which defines the standard dimer correlation length  $\xi$ , is twice as fast, i.e.

$$\tilde{\xi} = 2\xi. \quad (\text{A28})$$

This behavior has indeed been observed in the numerical studies in the main text.

## 2. Ground state degeneracy

It is well-known that the  $Z_2$  spin liquid has degenerate ground states in the thermodynamic limit on a cylinder or torus. For the cylindrical geometry studied here, two states are expected. Here we would like to understand the scaling of the gap between these two states, and also better understand their character. We will see that, as discussed e.g. in Ref.<sup>48</sup>, that the presence of gapped spin excitations (which carry non-zero

electric gauge charge) makes a *qualitative* difference in these properties. This means that models neglecting these excitations, in particular the very popular quantum dimer models, actually give *incorrect* or *non-generic* scaling for the finite-size quasi-degenerate gap.

Consider first the pure gauge theory, Eq. (A3), in which coupling to matter fields is neglected. The ground state degree of freedom may be regarded as the presence or absence of a vison through the hole in the cylinder. The presence of the vison itself is measured by the Wilson loop operator around the cylinder,

$$W = \prod_{y=1}^L \sigma_{xy;xy+1}^z. \quad (\text{A29})$$

A state with a  $Z_2$  vortex in it has  $W = -1$  and without has  $W = 1$ . However, the ground state will not be an eigenstate of  $W$ . In fact, consider the conjugate operator

$$Q = \prod_{x=1}^L \sigma_{xy;xy+1}^x. \quad (\text{A30})$$

This operator *commutes* with  $H$  defined in Eq. (A3), and so is a constant of the motion. The two degenerate ground states have  $Q = \pm 1$  (we can pick any  $y$ , since others are related by Eq. (A4)). Note that  $WQ = -QW$ , so an eigenstate of  $Q$  is a symmetric or antisymmetric combination of the  $W$  (vison) eigenstates. This indicates physically that the vison may tunnel through the cylinder, by moving (virtually) through the entire long length  $L_y$  from one end to another, thereby connecting the  $W = 1$  and  $W = -1$  states. The tunneling amplitude for this process is naturally expected to be exponential in the length of the event, so we postulate that the gap in this case is  $t_v \sim e^{-L_x/\xi_x}$ . This has been shown explicitly in many places in the literature.

This result is generic for the pure  $Z_2$  gauge theory, and continues to hold even if longer (but finite) range plaquette and electric field terms are included. It relies only on the fact that  $Q$  does not create any physical gauge flux through finite plaquettes. However, if a matter field (i.e. the spinons) is present, the result is modified. To see this, let us imagine more carefully integrating out the spinons in going from Eq. (A1) to Eq. (A3), for the case of a cylinder of finite circumference. Then we will obtain not only contributions from small loops (which renormalize  $K$  etc.), but also, occurring first at  $O(t^{L_y})$ , contributions from loops which encircle the cylinder. Keeping just the leading of these terms, we have the slight modification of Eq. (A3)

$$H = -K \sum_{\square} \prod_{\langle ij \rangle \in \square} \sigma_{ij}^z - t_s \sum_x \prod_{y=1}^{L_y} \sigma_{xy;xy+1}^z - h \sum_{\langle ij \rangle} \sigma_{ij}^x, \quad (\text{A31})$$

where we expect  $t_s \sim e^{-L_y/\xi_y}$ , which physically is related to the amplitude for a virtual spinon to encircle the cylinder. Note that in this case  $Q$  no longer commutes with  $H$ , and the nature of the eigenstates is no longer clear. Now if we assume  $t_s \ll K, h$  and that for  $t_s = 0$  we are in the deconfined  $Z_2$

phase, we can project the Hamiltonian on the low-energy sector of the pure gauge theory, i.e. the two level system of the quasi-degenerate states. Then we obtain the effective Hamiltonian, written in a pseudo-spin notation in which  $\mu^z = \mp 1$  correspond to the vison/no-vison states:

$$H_{deg} = -t_v \mu^x - t_s L_x \mu^z. \quad (\text{A32})$$

Since  $t_v \sim e^{-L_x/\xi_x}$  and  $t_s \sim e^{-L_y/\xi_y}$ , the nature of the ground state depends crucially on the aspect ratio of the cylinder. For a fat cylinder, with small  $L_x/L_y$ , for which  $t_s \ll t_v$ , the eigenstates will be like those of the pure gauge theory, and the gap will be exponentially small in  $L_x$ .

However, for a ‘‘long’’ cylinder, with larger  $L_x/L_y$ , the gap will be exponential instead in  $L_y$ . Indeed, strictly in the limit of large  $L_x$  and  $L_y$  fixed, the higher energy state can no longer be regarded as quasi-degenerate: its energy, relative to the ground state, grows linearly with  $L_x$ , and so other states with local, non-topological excitations will have lower energy. The conditions for  $t_s$  to dominate are much less restrictive than this, however, requiring only  $t_s L_x \gg t_v$ , or  $\exp(L_x/\xi_x - L_y/\xi_y) \gg 1/L_x$ . In this limit, the ground state is an approximate eigenstate of  $\mu^z$ , i.e. a state of definite vison

number. Because of the quasi-one-dimensional nature of the DMRG technique, in the most effective regime of this technique, this is the expected form of the ground state. Note again that this regime is missed by the pure gauge theory and also the quantum dimer model.

The nature of the absolute ground state obtained by DMRG has implications for the entanglement entropy. As shown recently by Zhang *et al*<sup>49</sup>, the topological entanglement entropy for a cut with non-trivial topology actually depends upon the choice of quasi-degenerate wavefunction. The cylindrical cut studied here is precisely such a cut. The results of Ref.<sup>49</sup> imply that the topological entanglement entropy reaches its maximum and universal value (of  $-\ln 2$ ) when the ground state is a vison eigenstate, and takes a smaller (in magnitude) value for other superpositions of states, *vanishing* for the case of a vison superposition, as is obtained in the absence of spinons. Thus the result of our numerical study in the main text, in which we found rough agreement with the  $-\ln 2$  value for the topological entanglement entropy, in fact is evidence for such a vison eigenstate in the numerics, consistent with the predicted effects of virtual spin fluctuations.